Applied Catalysis B: Environmental 239 (2018) 168–177

Contents lists available at ScienceDirect

Applied Catalysis B: Environmental

journal homepage: www.elsevier.com/locate/apcatb

Temperature-programmed plasma surface reaction: An approach to determine plasma-catalytic performance

Alexander Parastaev[a], Wilfred F.L.M. Hoeben[b], Bert E.J.M. van Heesch[b], Nikolay Kosinov[a], Emiel J.M. Hensen[a,*]

[a] Inorganic Materials Chemistry Group, Eindhoven University of Technology, 5600 MB Eindhoven, The Netherlands
[b] Electrical Energy Systems Group, Eindhoven University of Technology, 5600 MB Eindhoven, The Netherlands

ARTICLE INFO

Keywords:
Non-thermal plasma
Heterogeneous catalysis
CO_2methanation
TPR
Ceria-zirconia

ABSTRACT

Plasma-enhanced heterogeneous catalysis offers a promising alternative to thermal catalysis due to the synergy between the plasma and the solid catalyst. However, there is only a limited mechanistic insight about the interactions of highly energetic electrons and excited molecules with heterogeneous catalysts in plasmas. Accurate performance comparison in a plasma-catalytic setting is complicated because of the intricate nature of the plasma-catalyst system: simultaneous reactions occurring in the gas-phase and at the catalytic surface; the dependence of the discharge on dielectric properties of the packed catalyst bed; and the dependence of permittivity and polarization of the catalyst on plasma parameters. Here, we present a method of temperature-programmed plasma surface reaction (TPPSR) that allows decoupling gas-phase processes from the surface plasma-induced reactions. Using this method we reveal the main reasons of apparent synergy between plasma and heterogeneous catalyst for the case of carbon dioxide hydrogenation. Experiments with isotopically labelled CO_2 and temperature-programmed plasma reaction experiments in flow of CO_2/H_2 prove a substantial role of gas-phase dissociation/hydrogenation for the observed catalyst activity and selectivity. The product distribution and reaction pathways do not significantly depend on the discharge parameters. Taking into account overheating of the catalytic bed for comparison of catalytic activity with and without plasma, it was concluded that energy dissipation also plays an important role. The observed plasma enhancement is in part due to the acceleration of electron-induced surface reactions.

1. Introduction

Catalytic hydrogenation of carbon dioxide to methane (the Sabatier reaction) is an important catalytic process. It is applied in the production of synthesis gas, the formation of compressed natural gas [1] and the purification of feedstock for the production of ammonia [2]. The two principle reactions involved are the direct methanation of carbon dioxide and the water-gas shift (WGS) reaction that converts carbon dioxide to carbon monoxide.

$$CO_2 + H_2 \leftrightarrow CO + H_2O \quad \Delta H_{298K} = 42.1\ kJ/mol \tag{1}$$

$$CO_2 + 4H_2 \leftrightarrow CH_4 + 2H_2O \quad \Delta H_{298K} = -165\ kJ/mol \tag{2}$$

Non-thermal plasma (NTP) is a promising medium in which to perform catalytic reactions such as CO_2 methanation. Collisions with high energetic electrons in NTP result in ionization and dissociation, and electronic, vibrational, and rotational excitation of neutral reactant molecules [3]. In addition, running a reaction in a plasma can help to overcome thermodynamic equilibrium limitations without heating the system [4]. Many researchers have reported a synergy between heterogeneous catalysts and non-thermal plasma for the reactions of CO_2 conversion. Nizio et al. studied the activity of CO_2 methanation at low temperature in a dielectric barrier discharge (DBD) reactor [5]. Bacariza et al. reported that the promotion of Ni/CsY catalyst with cerium oxide results in an enhanced dielectric properties and higher activity in CO_2 methanation [6]. Improved performance of a Ni/γ-Al_2O_3 catalyst in dry reforming of CH_4 in a low-temperature plasma was mentioned in another study [7]. Wang et al. observed a higher methanol yield in CO_2 hydrogenation over a Cu/γ-Al_2O_3 catalyst in a tailor-made water-cooled DBD reactor at atmospheric pressure and room temperature [8]. Another recent study concerned the one-step plasma-assisted reaction of CO_2 and CH_4 in the presence of noble-metal catalysts, which resulted in enhanced yield of acetic acid, ethanol and methanol [9].

Current mechanistic understanding of the synergy between

* Corresponding author.
E-mail address: e.j.m.hensen@tue.nl (E.J.M. Hensen).

https://doi.org/10.1016/j.apcatb.2018.08.011
Received 8 June 2018; Received in revised form 24 July 2018; Accepted 3 August 2018
Available online 04 August 2018

heterogeneous catalysts and plasma is very limited. The main challenge is to meaningfully compare catalyst performance in different plasma operation modes and also different catalysts in a plasma. This is difficult because the properties of plasma depend on the filling material (*e.g.*, increasing the dielectric constant enhances the electric field) [10], while the permittivity and polarization of the catalyst is determined by the plasma parameters. Furthermore, unlike in conventional heterogeneous catalysis, comparison of catalysts used in a plasma is complicated by the simultaneous occurrence of reactions at the catalyst surface and in the plasma.

Comprehensive experimental and computational investigation of plasma-catalytic systems is required to gain a better understanding of the interaction between the plasma and the solid catalyst. A number of novel advanced techniques have recently been developed in this area. Isotopically-labeled oxygen was used to study the role of oxygen species in plasma-driven catalysis of volatile organic compound (VOC) oxidation [11]. NTP was found to lead to enhanced interaction of oxygen with the catalytic surfaces. Another technique applied to investigate the speciation of surface intermediates in conventional and plasma-catalysis is *operando* FTIR. Several FTIR studies were dedicated to the mechanism of plasma-assisted iso-propanol oxidation over γ-Al_2O_3 [12], selective catalytic reduction of NO_x [13], VOC removal from air over γ-Al_2O_3, TiO_2, and CeO_2 [14], CO_2 methanation over Ni-USY in different configurations (in-plasma catalysis and post-plasma catalysis) and with microsecond time-resolved spectroscopy [15,16]. Electron paramagnetic resonance (EPR) spectroscopy has been applied as an appropriate method to detect radical species formed by the NTP as well as chemical changes of the catalyst [3]. Pre-adsorption of different adsorbates followed by treatment in plasma has also been applied to distinguish the reactivity of gas-phase species and those adsorbed on the surface of the catalyst. This method was effective for studying oxidation of VOCs such as iso-propanol [17,18], toluene and propane [19]. Regeneration of MnO by direct thermal treatment, ozonolysis prior to thermal treatment and *in situ* non-thermal plasma prior to thermal treatment was studied as well [20]. Next to such experimental approaches, computational studies of the interaction between NTP and catalysts are also becoming important to obtain better insight into the reaction mechanism [21].

A well-known complication in plasma-catalysis involves catalyst overheating, which strongly affects the evaluation of plasma-catalytic performance. A dielectric barrier discharge (DBD) plasma can induce dielectric heating of the catalyst and in this way contribute to a higher apparent catalytic activity. Lee et al. reported that the enhancement of CO_2 methanation rate in the presence of a Ru/γ-Al_2O_3 catalyst occurred by electron collisions and dielectric heating from a DBD plasma. It was concluded, however, that electron collisions were a major contributor, because the catalytic activity in the plasma was higher than at the same temperature without discharges [22]. A recent study by Gibson et al. described a plasma-catalyst synergy for CH_4 oxidation using extended X-ray absorption fine structure (EXAFS) spectroscopy. No significant structural changes of the catalyst were observed. However, the change of the mean-squared thermal disorder parameter (σ^2) was used to determine the actual temperature of Pd nanoparticles. Although the NTP led to heating of Pd nanoparticles, their temperature was lower than the temperature required for the thermal CH_4 oxidation reaction [23]. One drawback of this EXAFS-based approach is the necessity to use synchrotron radiation. A more convenient but nonetheless expensive method is IR thermography. An IR camera in combination with a sapphire DBD reactor was used by Nozaki et al. to evaluate thermal and non-thermal effects of a non-equilibrium plasma [24]. Trinh et al. showed that long-lived ozone species play a dominant role in the plasma-catalytic oxidation of ethylene taking into account the plasma-induced overheating up to a temperature of 135 °C [25].

Overall, novel characterization methods and approaches to compare catalytic performance have to be developed in order to understand the synergism in plasma-catalysis. Here, we present a method called temperature-programmed plasma surface reaction (TPPSR), which is designed to decouple gas-phase processes in a plasma from the processes at the catalyst surface and to properly compare the performance of plasma-catalytic systems. We apply this method and a more conventional temperature-programmed plasma reaction (TPPR) to study the methanation of CO_2. The approach is to first adsorb the CO_2 reactant on the catalyst surface, followed by temperature ramping in a plasma containing H_2. Conversion processes in the plasma are minimized because the majority of the reacting species are adsorbed on the catalyst surface. In order to validate this approach, we also carried out experiments where isotopically labelled CO_2 was adsorbed on the catalyst and the temperature-programmed reaction was carried out in a mixture of non-labelled CO_2 and H_2.

2. Experimental

2.1. Catalyst preparation

All chemicals were obtained from Sigma-Aldrich: cobalt nitrate hexahydrate, copper nitrate trihydrate, and nanopowder $CeZrO_4$. A series of $CeZrO_4$ based catalysts with different metals were prepared using a wet impregnation method. For this purpose, the desired amount of metal nitrates were dissolved in 50 ml of deionized water. The suspension obtained by adding 2 g of nanocrystalline $CeZrO_4$ was stirred for 2 h. Then, the water was removed in a rotary evaporator. The catalysts were dried at 110 °C in air overnight and then calcined at 350 °C for 4 h. The catalyst powder was pelletized, crushed and sieved in order to obtain homogeneous fraction of 125–250 µm. Prior to catalytic activity tests the catalysts were reduced at 450 °C in H_2 for 4 h.

2.2. Catalyst characterization

The crystalline structure of the catalysts was determined by recording XRD patterns with a Bruker D4 Endeavor diffractometer using Cu Kα-radiation. The particle size was estimated using the Scherrer equation.

The metal content was determining using ICP-OES (Spectro CIROS CCD spectrometer). Prior to measurement, the samples were dissolved in a 1:2.75 (by weight) mixture of $(NH_4)_2SO_4$: (concentrated) H_2SO_4 and diluted with water.

H_2-TPR experiments were performed with a Micromeritics Autochem II 2920 instrument. Typically, 100 mg catalyst was loaded in a tubular quartz reactor. The sample was reduced in 4 vol.% H_2 in N_2 at a flow rate of 50 mL/min, while heating from room temperature up to 600 °C at a ramp rate of 10 °C/min.

2.3. Catalytic activity measurements

2.3.1. Experimental setup

All experiments were carried out in a tubular DBD reactor made of quartz. The outer diameter of the reactor was 14 mm and the inner diameter 10 mm. The discharge zone in the reactor was 80 mm long and the discharge gap 3 mm. A stainless-steel mesh wrapped around the reactor served as the ground electrode. The inner electrode was a stainless steel rod with a diameter of 4 mm. It was connected to a home-made high voltage microsecond pulsed power supply (discharge frequency [*f*, (s^{-1})] up to 1 kHz with variable pulse duration, voltage up to 20 kV). Plasma parameters were monitored by an oscilloscope (Tektronix TDS 2024C) equipped with a high-voltage probe (PVM-2, North Star) and a current probe (Model 6600, Pearson Electronics). A volume of 5 ml catalyst (125–250 µm fraction) was packed in the discharge region and held by quartz wool. A scheme of the plasma-catalytic setup is shown in Fig. S1.

A typical discharge pattern (applied voltage and discharge current) for the microsecond pulse source is shown in Fig. 1. Zoomed-in inset for the current waveform shows spikes, attributed to intense

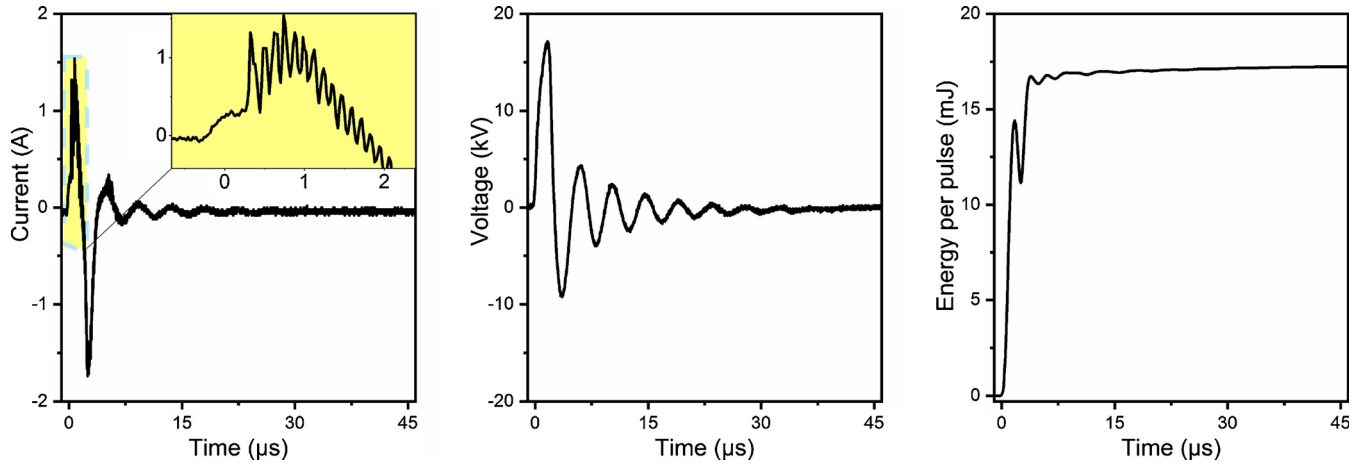

Fig. 1. Typical discharge patterns monitored by the oscilloscope and zoomed-in inset for the current waveform. Energy per pulse:15–20 mJ,10–1000 Hz,10–90 μs.

microdischarges observed in the empty DBD reactor. When a catalytic material is introduced inside the plasma reactor, the current waveform is changed significantly Fig. S2. Namely, the current waveform shows microdischarge activity with lower magnitude. In the packed-bed DBD reactor surface discharge and filamentary microdischarges can be generated simultaneously [26,27].

The voltage amplitude was kept constant and the pulse repetition rate was varied to change the energy density. The energy per pulse [E_p, (mJ)] is calculated by

$$E_p = \int_{pulse}^{0} V(t)I(t)dt \quad (1)$$

The energy density [ε, (kJ/mol)] was used as a parameter to compare the performance in terms of conversion and selectivity of CO_2 hydrogenation in a DBD reactor filled with catalyst with an empty DBD reactor. The energy density is defined as the energy deposited into the gas per unit volume and is calculated by

$$\varepsilon = \frac{fE_pV_m}{F} \bullet 10^{-6} \quad (2)$$

where F is the volumetric gas flow through the reactor (L/s) and V_m the molar volume of gas (22.4 L/mol at 0 °C).

2.3.2. Flow experiments

A variety of reaction experiments with different feed mixtures were performed to investigate the performance of the plasma-catalytic system in CO_2 hydrogenation. In a typical flow experiment, the oven temperature was kept constant and the energy density of the plasma was varied. The pulse duration during the plasma experiments was 90 μs at a frequency 100–1000 Hz. The CO_2/H_2 ratio was 1/4 at a total flow rate of 25 ml/min.

We also compared the catalytic performance with (TPPR) and without (TPR) plasma. The catalyst was heated at a rate of 10 °C/min. The pulse duration during the plasma experiments was 90 μs at a frequency 1 kHz. The CO_2/H_2/Ar ratio was 1/4/10 at a total flow rate of 75 ml/min.

For experiments with isotopically labelled CO_2, $^{13}CO_2$ (99%, Eurisotop) was first pre-adsorbed on the catalyst followed by flushing with a $^{12}CO_2$/Ar mixture. This was followed by a TPPR experiment in which we investigated the hydrogenation of gaseous $^{12}CO_2$ and adsorbed $^{13}CO_2$. In these experiments, the concentration of CO_2 in the gas phase was reduced to 0.3 vol% in order to minimize isotopic exchange.

2.3.3. Temperature-programmed plasma surface reaction

The TPPSR method (schematically shown in Fig. 2) consists of the following steps: (i) adsorption of the reactant on the catalyst surface at ambient temperatures; (ii) flushing of the reactor to remove gas-phase reactant molecules; (iii) exposure of the catalyst to the plasma at ambient temperature to remove weakly adsorbed species and (iv) heating the catalyst at a constant ramp rate in plasma, whilst following the catalytic performance by simultaneous gas-phase analysis by gas chromatography (Shimadzu GC-2014) and mass spectrometry (ThermoStar GSD 320 T2). In the present study, CO_2 was the reactant to be adsorbed on the catalyst, while H_2 was used as a feed during the plasma-catalytic step. The gas hourly space velocity (GHSV) during the adsorption step was set to 400 ml g^{-1} h^{-1} and during the TPPSR to 200 ml g^{-1} h^{-1}. The amount of CO_2 in the gas phase during a TPPSR experiment is much lower than in a conventional experiment when the reactant is part of the feed. Although plasma-induced or thermal desorption of the reactant can lead to a certain concentration of CO_2 in the gas phase as well, we expect the surface plasma-catalytic reactions to dominate the conversion processes during TPPSR experiments.

3. Results and discussion

3.1. Catalyst characterization

The XRD patterns of the $CeZrO_4$-supported catalysts are shown in Fig. 3. The diffraction peaks at 2θ = 29.2°, 33.8°, 48.7° and 57.7° correspond to the crystallographic (101), (002), (112) and (103) planes of $CeZrO_4$ (PDF No. 74–8060). This shows that the material is a homogeneous mixed solid oxide solution of Ce and Zr. Other diffraction peaks belong to copper oxide and cobalt oxide phases dispersed on the support. Using the Scherrer equation, we can estimate the crystallite size of copper oxide to be 28 nm. For 5% Co/$CeZrO_4$ and 20% Co/$CeZrO_4$ samples, the average cobalt oxide crystallite sizes are ~21 and ~25 nm, respectively. These results and the metal loadings as determined by elemental analysis are shown in Table 1. The crystallite size of the $CeZrO_4$ support was about 14 nm for all catalysts. However, on the TEM images acquired for these catalysts (Fig. S3), we can observe that the ceria-zirconia support has a broad particle size distribution up to about 50 nm. It was unfortunately not possible to image Co particles on the $CeZrO_4$ support by TEM because of the low contrast.

Fig. 4 shows the results of H_2-TPR characterization of the catalysts. For the copper sample, a significant H_2 consumption was observed at relatively low temperature around 150 °C and 220 °C. These results are in a good agreement with a previous report for the reduction of copper supported on ceria and ceria-zirconia [28]. The two reduction features can be attributed to reduction of highly dispersed copper strongly interacting with the support and a bulk copper oxide phase, respectively [29]. The reduction of cobalt catalysts correspond to very broad peaks centered around 420 °C with shoulders at lower temperature. Bulk Co_3O_4 reduction usually involves two steps, *i.e.* $Co_3O_4 \rightarrow CoO \rightarrow Co$.

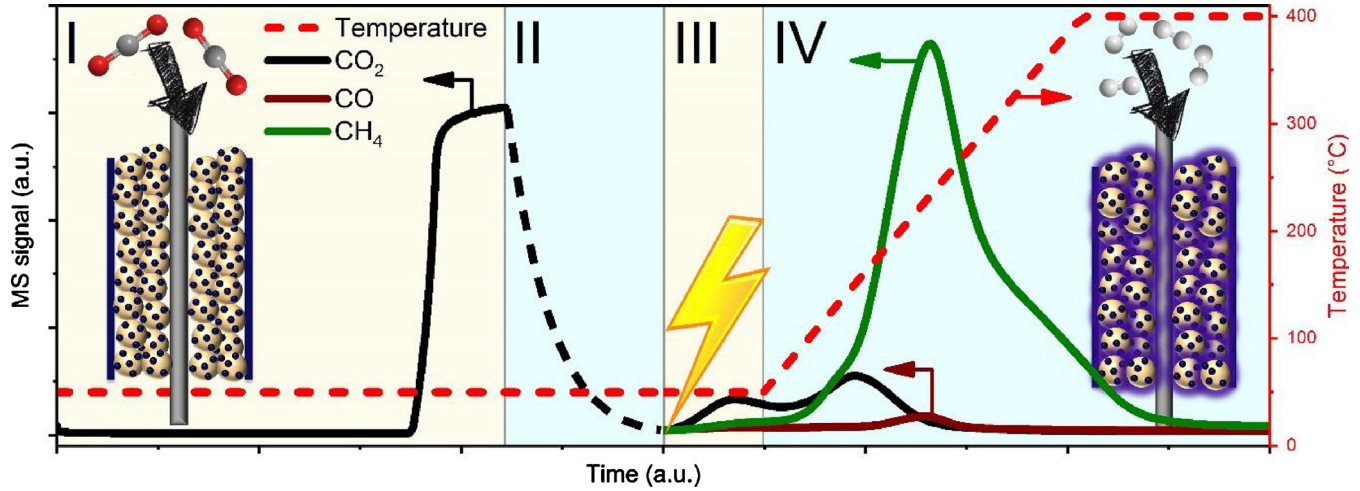

Fig. 2. Basic approach of the TPPSR method applied to the methanation of CO_2: (I) CO_2 is adsorbed on the catalyst by applying a constant 1% CO_2/Ar flow until complete breakthrough is observed; (II) flashing of the reactor with H_2 flow; after replacing the feed with H_2, the plasma is switched on followed by an isothermal period (III) and a temperature ramp (IV).

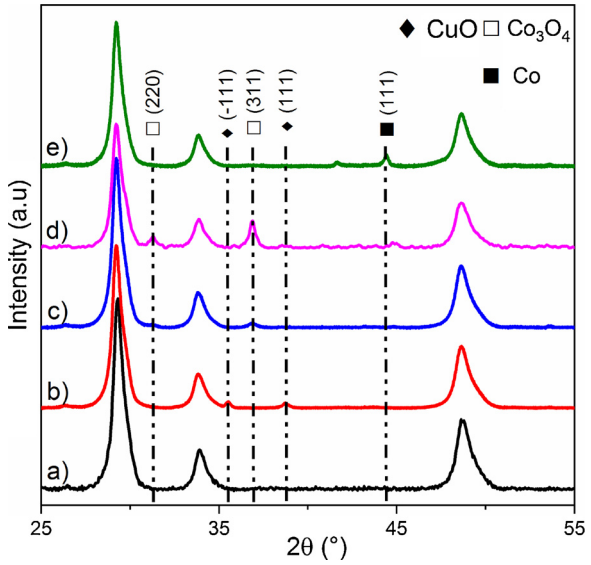

Fig. 3. XRD patterns of $CeZrO_4$-supported catalysts: a) $CeZrO_4$; b) 5% Cu/$CeZrO_4$; c) 5% Co/$CeZrO_4$; d) 20% Co/$CeZrO_4$ before reaction; and e) 20% Co/$CeZrO_4$ after reaction.

Table 1
Metal loadings and estimated particle size for different $CeZrO_4$-supported catalysts.

Catalyst	Metal loading[a] (%)	Particle size[b] (nm)
$CeZrO_4$	0	
5 % Cu/$CeZrO_4$	5.0	28
5 % Co/$CeZrO_4$	4.8	21
20 % Co/$CeZrO_4$	20.1	25
20 % Co/$CeZrO_4$ after reaction	–	35

[a] Determined by ICP.
[b] Determined by XRD.

The reduction of supported cobalt nanoparticles typically occurs between 300 °C and 400 °C. The higher reduction temperature observed for Co/$CeZrO_4$ likely relates to strong cobalt-support interactions [30].

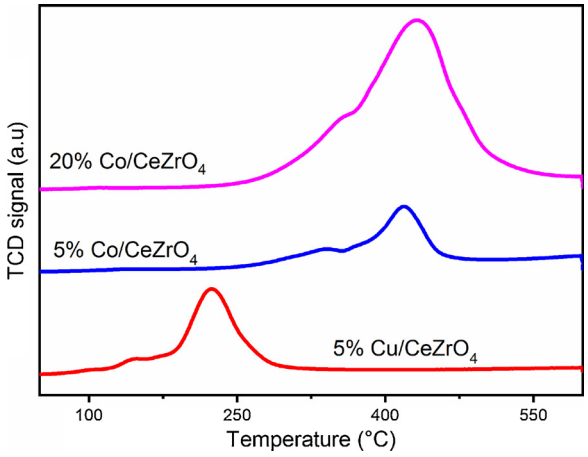

Fig. 4. TPR profiles of the $CeZrO_4$-supported catalysts.

3.2. Catalytic activity measurements

3.2.1. Flow experiments

As a reference case, we first studied the plasma-assisted hydrogenation of CO_2 in a DBD reactor, which was either empty or filled with $PbTiO_3$. The reaction was carried out at 150 °C to avoid condensation of produced water in the system (Fig. 5). The CO_2 conversion was not observed in the absence of plasma. The CO_2 conversion in the plasma increased proportionally to the energy density. The highest conversion of ~15% was reached at a frequency of 1 kHz, which corresponds to an energy density of 750 kJ/mol. It is known that conversion and energy efficiency of plasma-catalytic processes can be improved by filling the discharge gap of a DBD reactor with a ferroelectric material, because high dielectric constant leads to the enhancement of the electric field strength [31]. As CO_2 does not adsorb strongly on $PbTiO_3$, most of the reaction will occur in the gas phase. CO_2 methanation was not observed in the empty reactor nor in the reactor filled with $PbTiO_3$ (Fig. 5a) and the only products were CO and H_2O.

We then used a 5% Co/$CeZrO_4$ sample as the catalyst for CO_2 hydrogenation. Without plasma, the conversion was about 1% at 150 °C (Fig. 5b). In the plasma, it was found that the CO_2 conversion increased with the energy density. The highest CO_2 conversion was 70% at a frequency of 1 kHz (energy density of 750 kJ/mol). CH_4 was in all cases the main product with a selectivity above 75%. At the highest energy density, the CH_4 selectivity was nearly 100%. Similar results were

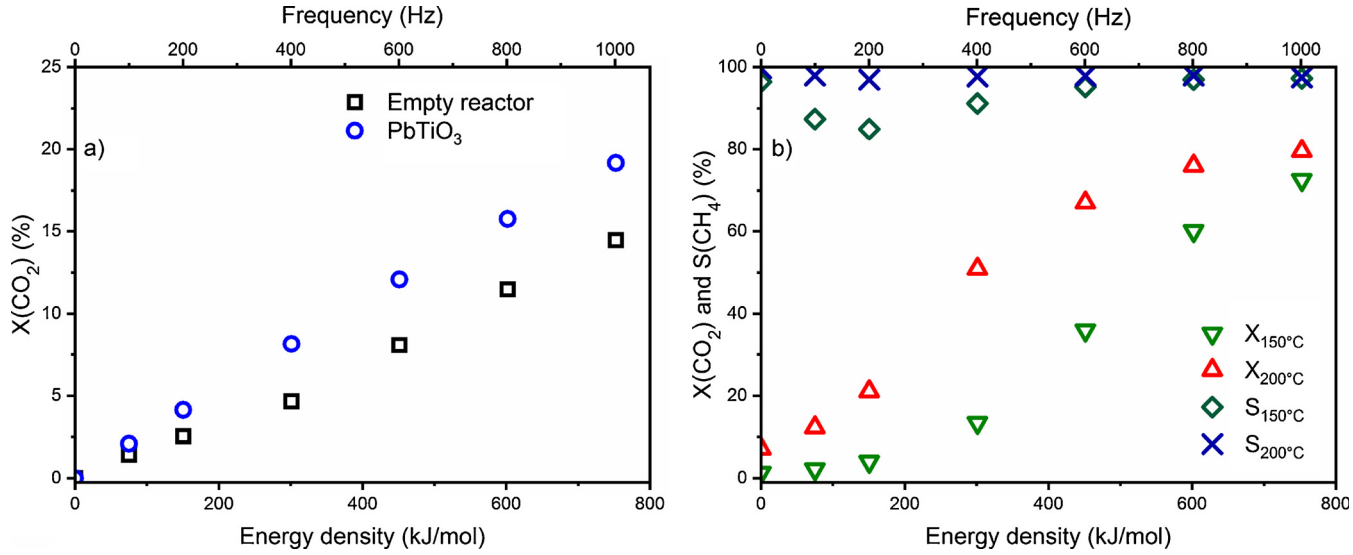

Fig. 5. Conversion (X) and selectivity (S) of CO_2 hydrogenation as a function of the energy density: a) CO_2 hydrogenation in an empty DBD reactor and in the presence of $PbTiO_3$ at 150 °C; b) CO_2 hydrogenation in the presence of 5% $Co/CeZrO_4$ at 150 °C and 200 °C.

obtained at 200 °C and very high selectivity to CH_4 was achieved for all values of the energy density.

The synergy between the catalyst and the plasma evident from Table 2 is in line with previous reports [5,8,9]. It results in higher CO_2 conversion at comparable CH_4 selectivity. There are several reasons for these synergetic effects such as plasma-enhanced surface reactions due to high-energy electrons, electric field and radicals on the surface [32]. Another possible explanation relates to processes occurring in the gas phase, for example, dissociation, excitation, ionization of reactants and products [3]. Finally, we should also take into account energy dissipation, which leads to overheating of the catalyst.

3.2.2. TPPR in $^{12}CO_2/H_2$

In general, TPR is a versatile method to characterize catalytic reactions, for it allows direct comparison of catalysts based on conversion and selectivity as a function of temperature [33]. Here we compared the performance of a 5% $Co/CeZrO_4$ catalyst in CO_2 methanation in a conventional TPR experiment and a similar experiment with the plasma switched on (TPPR). In both cases, the gas feed consisted of a CO_2/H_2/Ar mixture. For TPPR, we kept the catalyst first at 50 °C in the plasma before the heating was started in order to observe the impact of the plasma on the catalyst.

The TPR and TPPR results are shown in Fig. 6. In TPR, a broad CO_2 desorption peak at 100 °C is observed. CO_2 reduction starts at 250 °C and CH_4 and H_2O are the predominant reaction products. The trace for H_2O is shifted to higher temperatures in comparison to the CH_4 trace, because H_2O interacts stronger with the catalyst surface. A small amount of CO is also observed at higher temperature.

In TPPR, there is a sharp peak of CO_2 desorption when the plasma is ignited. At the same time, CO formation is observed. It is much higher than for flow experiments at 150 °C and 200 °C in the Section 3.2.1, because at 50 °C methanation activity is low. We attribute CO formation to the dissociation of CO_2 in the gas phase, because CO was also detected as the main product in plasma experiments in the same DBD reactor with and without $PbTiO_3$. In TPPR, a small amount of H_2O was observed at 50 °C. As low-temperature H_2O formation was not observed in experiments without plasma and H_2O strongly interacts with the $CeZrO_2$ support, we infer that H_2O is formed due to the reverse water-gas shift reaction on cobalt nanoparticles. Plasma-catalytic enhancement of reverse water-gas shift may be related to dissociation of CO_2 in the plasma.

Comparison of the TPR and TPPR profiles shows that the use of a plasma shifts the temperature of CH_4 formation to lower temperature (from 250 °C to 50 °C). The CH_4 TPPR profile also contains a shoulder in the 50–100 °C range (marked area in Fig. 6b). We link this to the facile formation of CO in the gas phase, which can be formed even in an empty DBD reactor, and its re-adsorption on cobalt nanoparticles leading to further hydrogenation to CH_4.

Table 2
Synergy for plasma-catalytic CO_2 hydrogenation at 150 °C in the presence of 5% $Co/CeZrO_4$ and performance of an empty DBD reactor and catalyst alone at the same conditions.

Filling material	Energy density (kJ/mol)	CO_2 conversion (%)	CH_4 selectivity (%)
Empty	750	15	0
5% $Co/CeZrO_4$	0	1	95
5% $Co/CeZrO_4$	750	70	99

3.3. TPPR in $^{12}CO_2/H_2$ with pre-adsorbed $^{13}CO_2$

Fig. 7a shows the results of an experiment in which $^{13}CO_2$ was pre-adsorbed on a $Co/CeZrO_4$ catalyst followed by temperature-programmed reaction in $^{12}CO_2/H_2$. During the initial isothermal period (50 °C), no $^{13}CH_4$ was observed. Formation of $^{13}CH_4$ was seen above 100 °C. On the other hand, $^{12}CH_4$ was immediately observed in the reactor effluent when the plasma was ignited. This indicates that methanation occurs mainly due to the conversion of gaseous CO_2. We speculate that CO_2 is converted into CO in the gas phase. As CH_4 was not observed in a plasma experiment with an empty DBD reactor nor in a plasma experiment with the $CeZrO_4$ support, we infer that CO is converted on cobalt nanoparticles. This result also implies that the reaction of CO on cobalt is facilitated by the plasma at low temperature.

Next, we performed a kinetic analysis for the formation of $^{12}CH_4$ and $^{13}CH_4$. For this we used leading edge analysis method as introduced by Habenschaden and Küppers [34]. It allows the determination of the activation energy using the leading edge of the temperature-programmed trace. From Fig. 7b, it can also be seen that the apparent activation energies for $^{12}CH_4$ and $^{13}CH_4$ formation are similar. This indicates that these products are formed *via* the same pathway when heating is applied. Therefore, the predominant pathway for plasma-catalytic CO_2 methanation *via* gas-phase CO was observed only in the isothermal regime at 50 °C.

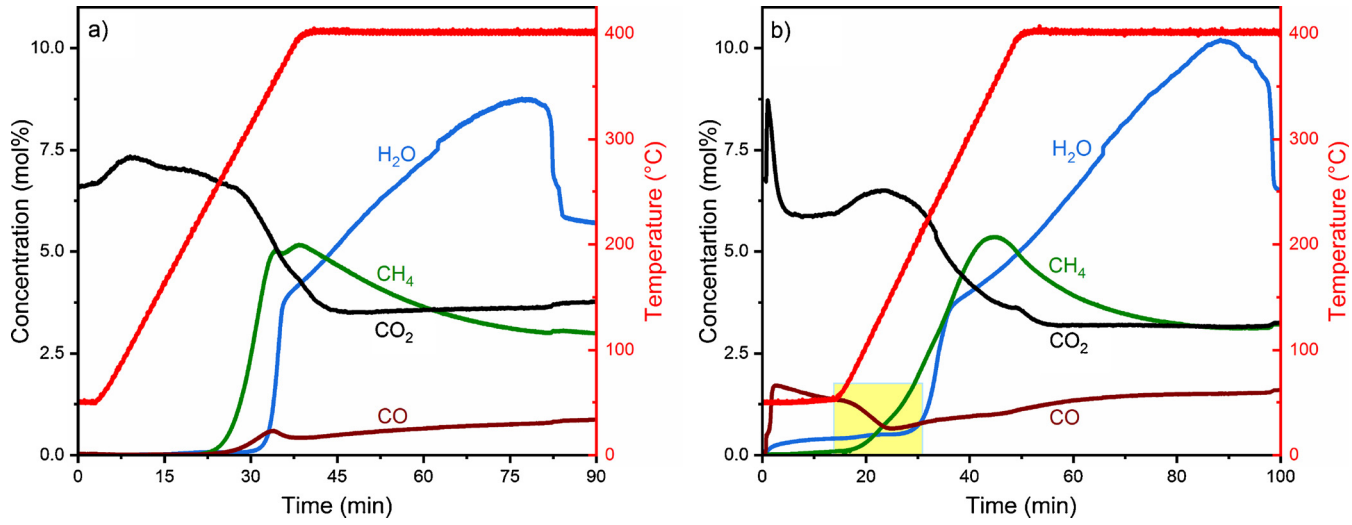

Fig. 6. CO_2 hydrogenation in the presence of 5% $Co/CeZrO_4$ catalyst by TPPR method: a) without plasma; b) in plasma, pulse duration 90 μs, frequency 1 kHz. $CO_2/H_2/Ar$ = 1/4/10, total flow 75 ml/min, heating ramp 10 °C/min.

3.4. TPPSR with pre-adsorbed $^{12}CO_2$

Next, we performed TPPSR in a H_2 flow with catalysts on which CO_2 was pre-adsorbed. This refers to the experiment sketched in Fig. 2.

Table 3 shows that the amount of CO_2 pre-adsorbed as determined from the breakthrough curves was similar for all three samples. This indicates that CO_2 adsorption mostly takes place on the support. Fig. 8 shows product formation as a function of time during the TPPSR experiment for $CeZrO_4$, 5% $Co/CeZrO_4$ and 5% $Cu/CeZrO_4$. For $CeZrO_4$, we observe that ignition of the plasma leads to desorption peaks of a CO_2 and CO. As CO_2 and CO desorption are nearly instantaneous, it is not likely that these features are due to heating of the catalyst. Instead, we attribute these desorption features to electron impact on the catalyst surface. Adsorption of CO_2 on $CeZrO_4$ materials will lead to the formation of various carbonates and formate species [35,36]. Their dissociation upon electron impact may lead to CO_2 and CO. Although it is also possible that CO is formed by plasma conversion of desorbed CO_2, Fig. 5a shows that the conversion of CO_2 to CO in a similar plasma is much lower than in the experiment in Fig. 8a. When the temperature is raised, a new CO_2 desorption feature is seen. The amount of CO is much lower, suggesting that most of the formates have already been decomposed at this stage. Above 275 °C, CO formation commences, which is likely due to reverse water-gas shift catalyzed by the $CeZrO_4$ surface. There are only very small amounts of CH_4 formed in the isothermal regime and around 400 °C.

Table 3
Mass balance and product distribution for the TPPSR catalysts screening. Pulse duration 90 μs, frequency 1 kHz, heating ramp 10 °C/min.

Catalyst	Results of breakthrough adsorption of CO_2 (mmol/g)	Mass balance (%)	Reactor outlet composition (%)		
			CO_2	CO	CH_4
$CeZrO_4$	0.160	66	66	31	3
5% Cu/$CeZrO_4$	0.157	75	32	43	25
5% Co/$CeZrO_4$	0.161	89	9	3	88

When the same experiment is done with 5%$Cu/CeZrO_4$, three CO_2 desorption peaks are observed. The amount of CO_2 and CO desorbed in the isothermal regime is lower than for $CeZrO_4$, which might be due to the stronger binding of carbonates and formates close to the Cu nanoparticles. Further CO_2 desorption occurs in two steps. This can be

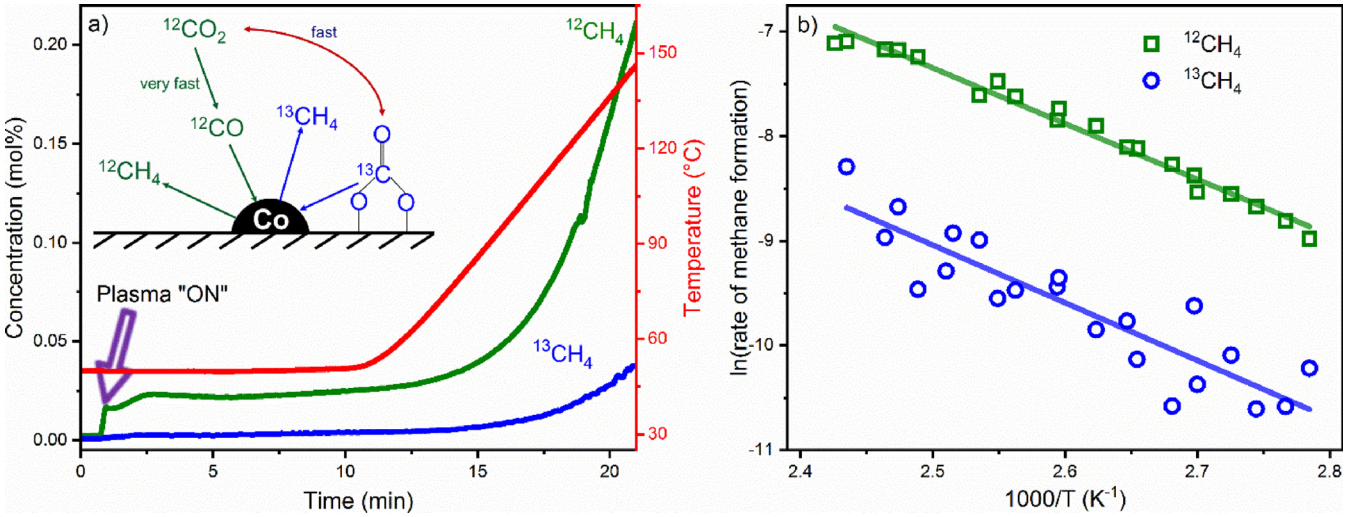

Fig. 7. Temperature-programmed hydrogenation of a feed of $^{12}CO_2/H_2/Ar$ (volumetric ratio: 1/100/275; flow rate 75 ml/min) on 5% $Co/CeZrO_4$ on which $^{13}CO_2$ was pre-adsorbed. The heating rate was 10 °C/min. The pulse duration was 90 μs at a frequency of 1 kHz, resulting in an energy density of 700 kJ/mol.

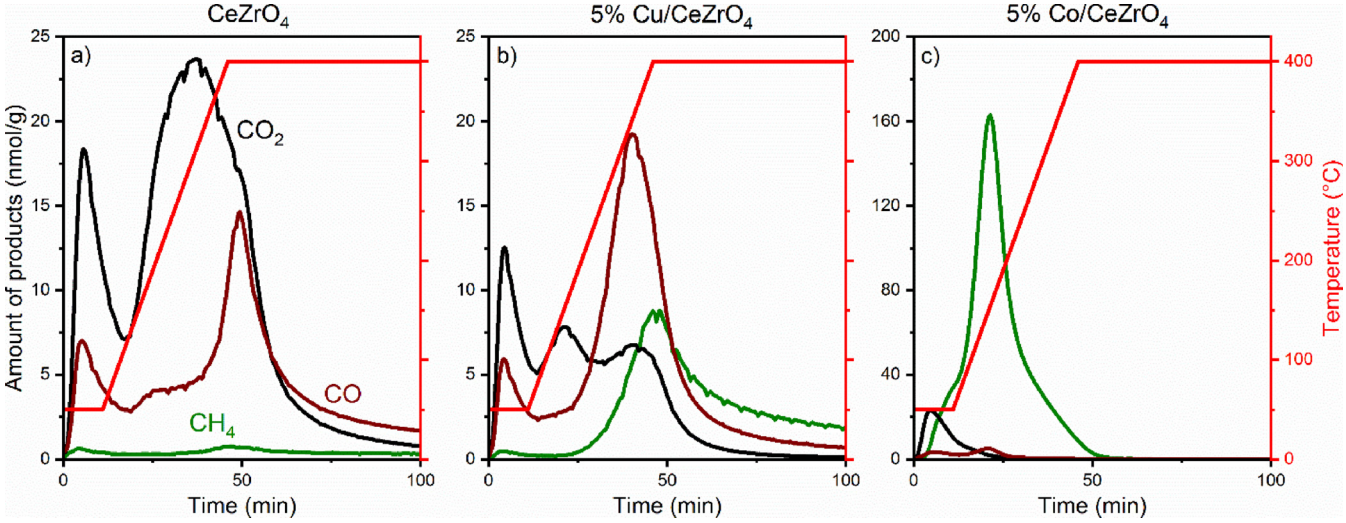

Fig. 8. TPPSR of CO_2 adsorbed on different $CeZrO_4$-based samples in a H_2 flow: $CeZrO_4$, 5% $Cu/CeZrO_4$ and 5% $Co/CeZrO_4$ at an energy density of 740 kJ/l.

explained as follows. The onset of the first peak during the temperature ramp is the same as for $CeZrO_4$. However, CO_2 will be converted *via* reverse water-gas shift to CO at lower temperature on $Cu/CeZrO_4$ than on $CeZrO_4$. We expect that this conversion is predominantly due to the conversion of carbonates and formates close to Cu particles. This can explain the second desorption peak during the temperature ramp, which is due to carbonate decomposition from parts of the surface where no Cu particles are in close proximity. CH_4 is also formed above 200 °C and the CH_4 trace shows a maximum around 375 °C. The overall CH_4 selectivity for 5% $Cu/CeZrO_4$ is ~25%, which is much higher than for $CeZrO_4$. The difference is due to the presence of copper metal.

With 5% $Co/CeZrO_4$ as the catalyst, CH_4 becomes the dominant reaction product. Whilst CO_2 and CO desorption are observed in the isothermal regime, CH_4 formation already commences at this stage. As already suggested by the results in Section 3.3, this finding implies that CO dissociation and hydrogenation can proceed during the plasma-catalytic reaction. Nevertheless, we should point out that heating of the catalyst cannot be excluded at this stage. In particular, in both of these experiments it is seen that CH_4 formation is delayed compared to CO formation. In the temperature ramping regime, most of the adsorbed CO_2 is converted to CH_4. The CH_4 profile shows a maximum below 200 °C.

Furthermore, the TPPR method allows us to directly compare the activity (Fig. 8a–c) and selectivity (Table 3) of catalysts in a plasma environment. Expectedly, the use of the $CeZrO_4$ support does not lead to any appreciable CH_4 yield. The main product is CO and CO_2 conversion is rather moderate. $Cu/CeZrO_4$ exhibits some CH_4 selectivity above 350 °C with higher overall CO selectivity. The most effective catalyst for CO_2 methanation is $Co/CeZrO_4$ with a total CH_4 yield of *ca.* 90%. The higher activity of cobalt than copper is in line with known activity trends reported for the Sabatier reaction [1,2,37].

The TPPR method also allows studying the influence of the plasma parameters on the surface processes like plasma-induced desorption and comparing plasma-induced processes to conventional TPR. Fig. 9 shows a comparison between thermal and plasma-assisted desorption of CO_2. In a He flow CO_2 desorption profile has two broad features at 200 °C and 400 °C A small amount of CO is desorbed at 200 °C and 400 °C. Such strong adsorption can be attributed to the high oxygen storage capacity of $CeZrO_4$ [38]. Desorption profile of CO_2 in a H_2 flow (Fig. 9b) in the absence of plasma is similar to the experiment in a He flow. The CO_2 desorption peak is centered at 200 °C. Clearly, desorption of CO_2 at 50 °C in the presence of plasma was more pronounced. But the amount of desorbed CO_2 is much smaller compared to the experiment in He flow. Most of the strongly adsorbed CO_2 was reduced to CO_2 and CH_4.

Fig. 10 shows the effect of plasma discharge frequency on the catalytic performance of 5% $Co/CeZrO_4$ in CO_2 hydrogenation. The temperature maximum of CH_4 production (*i.e.*, catalytic activity) was shifted to significantly lower temperature with increasing discharge frequency. In literature, such an increase in activity upon plasma treatment is usually explained by electron-induced reactions, or the change of catalyst properties in the strong electric field and the formation of radicals on the catalyst surface. However, an effect of catalyst overheating in plasma cannot be eliminated at this stage.

Using the TPPR method, we could also nearly close the mass balance using the breakthrough curves of CO_2 and the total amount of reactants and products leaving the reactor. The adsorbed amounts of CO_2 for 5% $Co/CeZrO_4$ are displayed in Fig. S4 and similar for all experiments, implying high reproducibility of the measurements. The product distribution and the mass balance for the different experiments without and with plasma are shown in Fig. 10d as well. The identical product distribution in TPPR experiments at different discharge frequencies and without plasma indicates that the mechanism of surface reactions is not changed in a plasma environment, as compared to thermal catalysis. On the contrary, TPPR experiments in a flow of CO_2 and H_2 described in the Section 3.2.2 show significant differences in the product distribution, which proves that the products of plasma-catalysis are very strongly affected by chemical processes occurring in the plasma.

Catalysts with different metal loadings can be also compared by the TPPR method (Fig. 11). The maxima of CH_4 formation are shifted to the lower temperatures with increasing metal loading. This can be explained by the fact that CO_2 pre-adsorbed in close proximity to cobalt particles is easily hydrogenated. It has been shown that CO_2 can be activated on the ceria-zirconia support to form carbonates, which can be further hydrogenated using H atoms deriving from dissociative H_2 adsorption on the supported metal particles [36]. Therefore, a higher metal loading will favor the methanation reaction of adsorbed CO_2.

3.4.1. *CO hydrogenation followed by TPPR*

CO is an intermediate of CO_2 hydrogenation. It can be obtained either by reduction of CO_2 with H_2 on the catalyst surface or by plasma-induced dissociation in the gas phase. To better understand the role of CO during CO_2 hydrogenation, we performed TPPR experiments with pre-adsorbed CO.

Results depicted in Fig. 12 demonstrate that CO adsorbed on $Co/CeZrO_4$ and Co/SiO_2 can be easily hydrogenated in a plasma at a frequency of 1 kHz without external heating. A difference between silica and ceria-zirconia Co supported catalysts is the occurrence of a high-

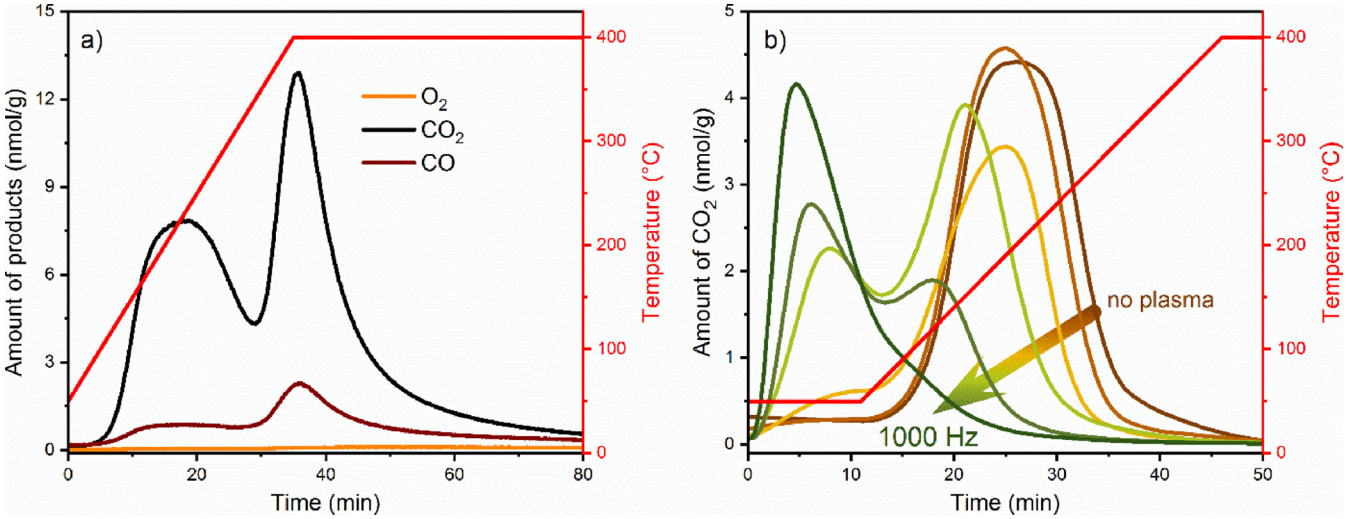

Fig. 9. a) CO_2 desorption profile without plasma in helium flow; b) CO_2 desorption profiles in hydrogen plasma under different conditions: 0, 100, 250, 500, 750, 1000 Hz. 5% $Co/CeZrO_4$ catalyst, pulse duration 90 μs.

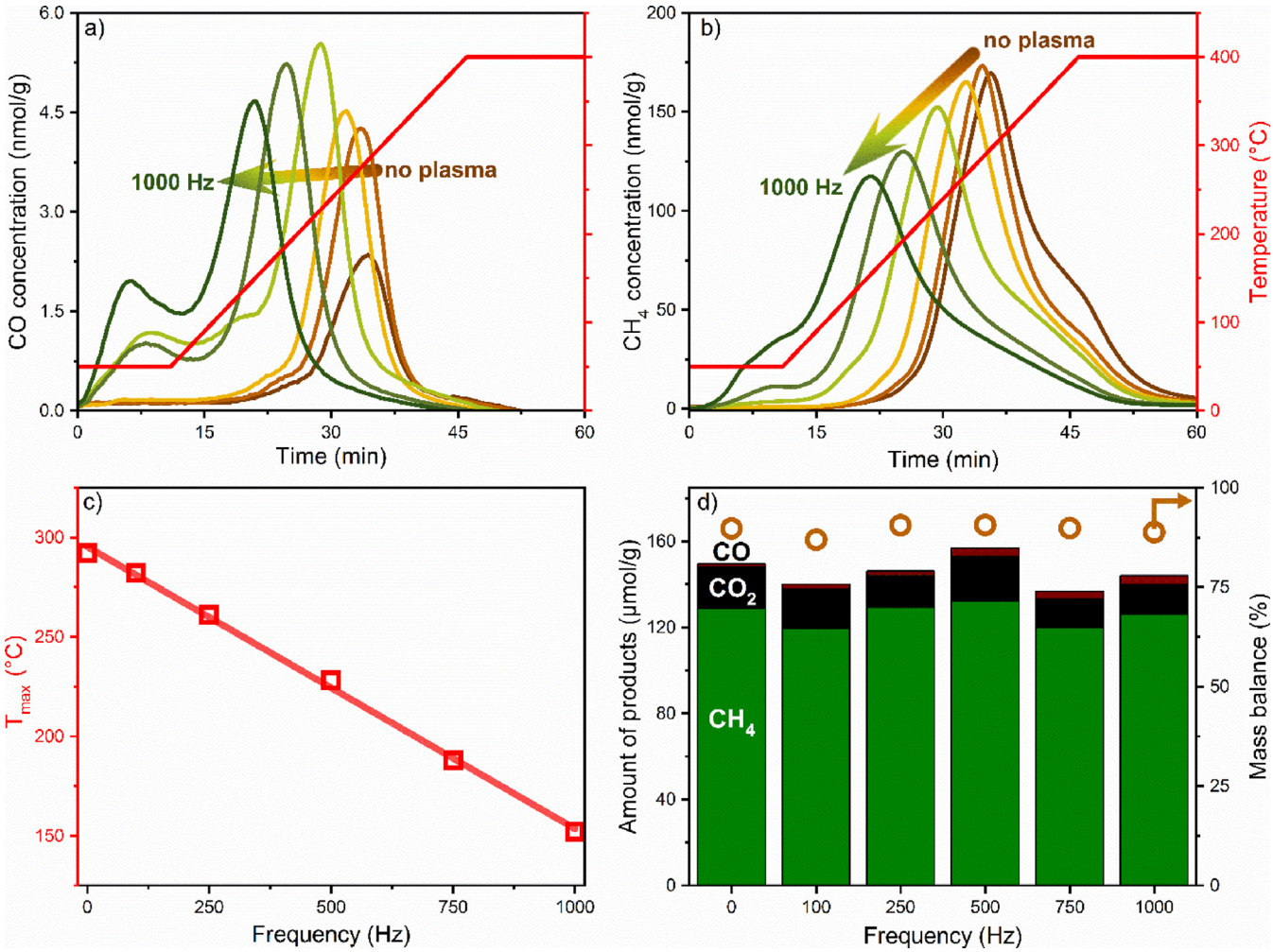

Fig. 10. a) and b) CO and CH_4 formation profile at different frequencies: 0, 100, 250, 500, 750 and 1000 Hz; c) Temperature of the maximum CH_4 formation profile; d) Product distribution and mass balance. Catalyst 5% $Co/CeZrO_4$, pulse duration 90 μs.

temperature feature for $Co/CeZrO_4$, which is most probably due to the formation of carbonates and/or formates strongly bound to the surface of the support. These surface-adsorbed species are the result of oxidative adsorption of CO. This high-temperature feature is absent for Co/SiO_2 because the silica support cannot form these species [36]. Therefore, we can assign the main feature of CH_4 formation, which does not depend on the support, to hydrogenation of CO on the Co metal. Finally, we note that the temperature maximum in CO hydrogenation

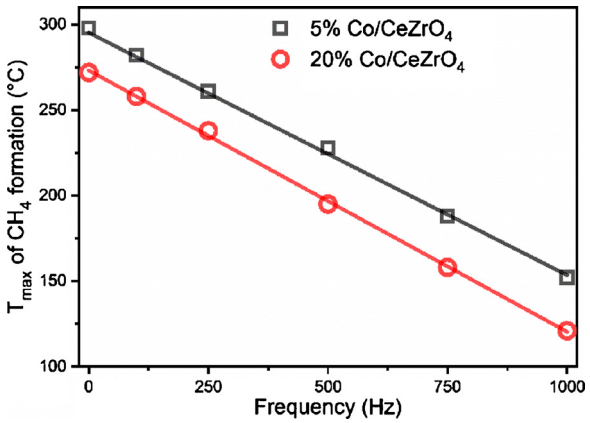

Fig. 11. Maximum temperature of CH_4 formation for CO_2 hydrogenation in the presence of 5% $Co/CeZrO_4$ and 20% $Co/CeZrO_4$ catalysts.

depends more strongly on temperature than the temperature maximum in CO_2 hydrogenation.

4. Temperature profiles

The DBD plasma can generally induce dielectric overheating of the catalyst particles and therefore increase the apparent catalytic activity. Some recent publications have described the effect of overheating in plasma-catalysis using an ethanol thermometer [25], XAFS spectroscopy [23], and infrared thermography [24]. To evaluate the impact of dielectric heating on the activity of the catalysts, we measured the temperature profiles by using a conventional thermocouple. We placed a thermocouple into the catalyst bed, and measured the temperature right after the plasma was switched off. A rather significant overheating of up to 100 °C was observed with plasma in the isothermal period (Fig. S5), while without plasma a certain constant lag (~40 °C) between the oven temperature and the actual bed temperature was observed. Nevertheless, the actual maximum of CH_4 production for conventional heating was approximately at 240 °C, while for the plasma-catalytic process it was about 200 °C, at least 40 °C lower (Fig. 13). Therefore, the observed synergy in plasma-catalytic methanation of CO_2 cannot be explained only by the overheating of the catalyst bed and an actual intrinsic positive effect of plasma is demonstrated. It should also be noted that above 250 °C the temperature with and without plasma is

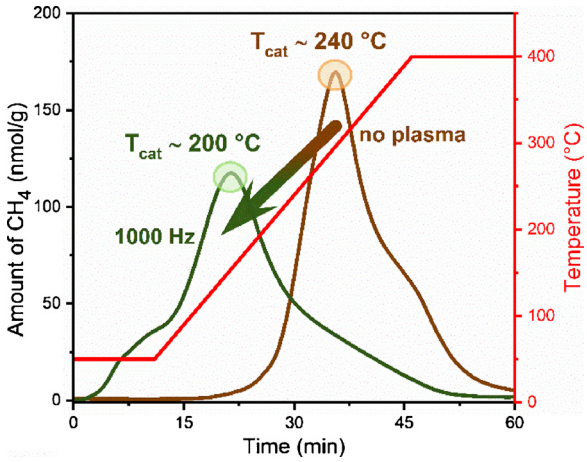

Fig. 13. Temperature measurements for CO_2 hydrogenation in the presence of 5% $Co/CeZrO_4$ with and without plasma.

fairly similar. The plasma-induced overheating effect in our DBD reactor mainly takes place in the range from 50 to 250 °C. In any case, temperature measurements for catalytic material in plasma are very important to distinguish the plasma-induced chemical effects and thermal catalysis. It is challenging to measure the temperature of the catalytic bed in a plasma because of limited options for temperature sensors suitable for the high-voltage environment. Moreover, insertion of any temperature sensor inside the plasma-catalytic bed will influence the electric field and discharge properties. Application of pyrometers is also complicated, because ceramic materials, mainly used for DBD reactor (quartz, alumina), are not transparent to the IR light. There is a clear need, therefore, to develop new methods for temperature measurements in plasma-catalytic settings.

5. Conclusions

A new TPPSR method to compare the performance of plasma-catalytic systems was presented. This method can provide a solid understanding of the plasma-catalyst interactions, which can facilitate further development of efficient plasma-catalytic processes. The approach should be applicable to a wide range of plasma-catalytic reactions, such as dry reforming, NO_x removal, VOC oxidation and CO_2 hydrogenation. Moreover, the influence of dielectric and adsorption properties of

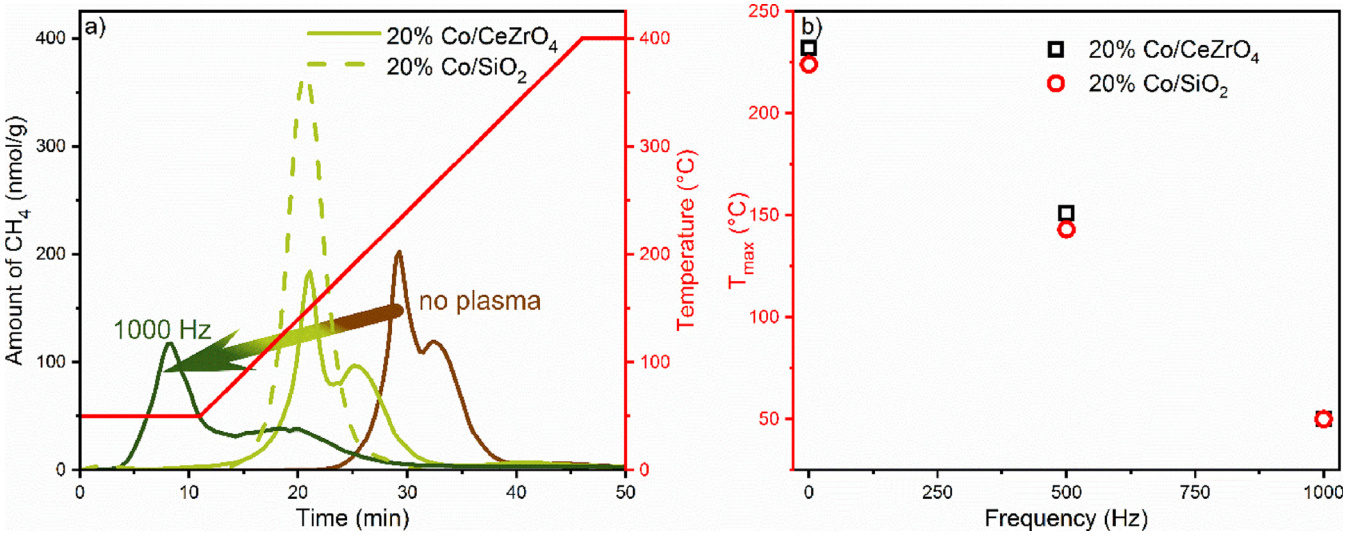

Fig. 12. CO hydrogenation in the presence of 20% $Co/CeZrO_4$ and 20% Co/SiO_2 catalysts by the TPPR method: a) TPPR profiles at different frequencies: 0, 500 and 1000 Hz; b) maximum temperatures of CH_4 formation. Pulse duration 90 μs.

catalytic materials and discharge parameters can be accurately compared with TPPSR. The main requirements for the design of meaningful TPPSR experiments are (i) to avoid extensive conversion of reactants in the gas phase and (ii) to ensure reasonable adsorption of at least one of the reactants on the catalytic surface. We illustrated the potential of TPPSR to decouple the gas-phase plasma processes and the surface plasma-induced reactions in CO_2 hydrogenation. Using TPPSR in combination with isotopically labelled CO_2, we could understand the role of surface and gas phase processes in Co and Cu catalyzed plasma-enhanced methanation and to assess the impact of plasma parameters on these process. We also emphasized the influence of plasma-induced overheating as a contributor to the enhanced performance. It was found that the plasma-induced gas-phase dissociation of CO_2 favors a low-temperature reaction pathway.

Acknowledgements

This research was supported by the Netherlands Organisation for Scientific Research (NWO)-Alliander Program on Plasma Conversion of CO_2 [Project number: 13583].

Appendix A. Supplementary data

Supplementary material related to this article can be found, in the online version, at doi: https://doi.org/10.1016/j.apcatb.2018.08.011.

References

[1] W. Wang, S. Wang, X. Ma, J. Gong, Recent advances in catalytic hydrogenation of carbon dioxide, Chem. Soc. Rev. 40 (2011) 3703–3727, https://doi.org/10.1039/c1cs15008a.
[2] W. Wang, J. Gong, Methanation of carbon dioxide: an overview, Front. Chem. Sci. Eng. 5 (2011) 2–10, https://doi.org/10.1007/s11705-010-0528-3.
[3] U. Roland, F. Holzer, A. Pöppl, F.-D. Kopinke, Combination of non-thermal plasma and heterogeneous catalysis for oxidation of volatile organic compounds: Part 3. Electron paramagnetic resonance (EPR) studies of plasma-treated porous alumina, Appl. Catal. B Environ. 58 (2005) 227–234, https://doi.org/10.1016/j.apcatb.2004.11.025.
[4] X. Tu, J.C. Whitehead, Plasma-catalytic dry reforming of methane in an atmospheric dielectric barrier discharge: understanding the synergistic effect at low temperature, Appl. Catal. B Environ. 125 (2012) 439–448, https://doi.org/10.1016/j.apcatb.2012.06.006.
[5] M. Nizio, A. Albarazi, S. Cavadias, J. Amouroux, M.E. Galvez, P. Da Costa, Hybrid plasma-catalytic methanation of CO_2 at low temperature over ceria zirconia supported Ni catalysts, Int. J. Hydrogen Energy 41 (2016) 11584–11592, https://doi.org/10.1016/j.ijhydene.2016.02.020.
[6] M.C. Bacariza, M. Biset-Peiró, I. Graça, J. Guilera, J. Morante, J.M. Lopes, T. Andreu, C. Henriques, DBD plasma-assisted CO_2 methanation using zeolite-based catalysts: structure composition-reactivity approach and effect of Ce as promoter, J. CO2 Util. 26 (2018) 202–211, https://doi.org/10.1016/J.JCOU.2018.05.013.
[7] Q. Wang, B.-H. Yan, Y. Jin, Y. Cheng, Dry reforming of methane in a dielectric barrier discharge reactor with Ni/Al_2O_3 catalyst: interaction of catalyst and plasma, Energy Fuels 23 (2009) 4196–4201, https://doi.org/10.1021/ef900286j.
[8] L. Wang, Y. Yi, H. Guo, X. Tu, Atmospheric pressure and room temperature synthesis of methanol through plasma-catalytic hydrogenation of CO_2, ACS Catal. 8 (2018) 90–100, https://doi.org/10.1021/acscatal.7b02733.
[9] L. Wang, Y. Yi, C. Wu, H. Guo, X. Tu, One-step reforming of CO_2 and CH_4 into high-value liquid chemicals and fuels at room temperature by plasma-driven catalysis, Angew. Chemie Int. Ed. 56 (2017) 13679–13683, https://doi.org/10.1002/anie.201707131.
[10] K. Van Laer, A. Bogaerts, Influence of gap size and dielectric constant of the packing material on the plasma behaviour in a packed bed DBD reactor: a fluid modelling study, Plasma Process. Polym. 14 (2017), https://doi.org/10.1002/ppap.201600129 1600129.
[11] H.-H. Kim, A. Ogata, M. Schiorlin, E. Marotta, C. Paradisi, Oxygen isotope ($^{18}O_2$) evidence on the role of oxygen in the plasma-driven catalysis of VOC oxidation, Catal. Lett. 141 (2011) 277–282, https://doi.org/10.1007/s10562-010-0491-0.
[12] M. Rivallan, E. Fourré, S. Aiello, J.-M. Tatibouët, F. Thibault-Starzyk, Insights into the mechanisms of isopropanol conversion on γ-Al_2O_3 by dielectric barrier discharge, Plasma Process. Polym. 9 (2012) 850–854, https://doi.org/10.1002/ppap.201200021.
[13] C.E. Stere, W. Adress, R. Burch, S. Chansai, A. Goguet, W.G. Graham, C. Hardacre, Probing a non-thermal plasma activated heterogeneously catalyzed reaction using in situ DRIFTS-MS, ACS Catal. 5 (2015) 956–964, https://doi.org/10.1021/cs5019265.
[14] A. Rodrigues, J.M. Tatibouët, E. Fourré, Operando DRIFT spectroscopy characterization of intermediate species on catalysts surface in VOC removal from air by non-thermal plasma assisted catalysis, Plasma Chem. Plasma Process. 36 (2016) 901–915, https://doi.org/10.1007/s11090-016-9718-1.
[15] F. Azzolina-Jury, D. Bento, C. Henriques, F. Thibault-Starzyk, Chemical engineering aspects of plasma-assisted CO_2 hydrogenation over nickel zeolites under partial vacuum, J. CO2 Util. 22 (2017) 97–109, https://doi.org/10.1016/j.jcou.2017.09.017.
[16] F. Azzolina-Jury, F. Thibault-Starzyk, Mechanism of low pressure plasma-assisted CO_2 hydrogenation over Ni-USY by microsecond time-resolved FTIR spectroscopy, Top. Catal. 60 (2017) 1709–1721, https://doi.org/10.1007/s11244-017-0849-2.
[17] L. Sivachandiran, F. Thevenet, P. Gravejat, A. Rousseau, Isopropanol saturated TiO_2surface regeneration by non-thermal plasma: Influence of air relative humidity, Chem. Eng. J. 214 (2013) 17–26, https://doi.org/10.1016/j.cej.2012.10.022.
[18] L. Sivachandiran, F. Thevenet, A. Rousseau, Isopropanol removal using Mn_xO_y packed bed non-thermal plasma reactor: comparison between continuous treatment and sequential sorption/regeneration, Chem. Eng. J. 270 (2015) 327–335, https://doi.org/10.1016/j.cej.2015.01.055.
[19] Y.-H. Song, S.-J. Kim, K.-I. Choi, T. Yamamoto, Effects of adsorption and temperature on a nonthermal plasma process for removing VOCs, J. Electrostat. 55 (2002) 189–201, https://doi.org/10.1016/S0304-3886(01)00197-8.
[20] L. Sivachandiran, F. Thevenet, A. Rousseau, Regeneration of isopropyl alcohol saturated Mn_xO_y surface: comparison of thermal, ozonolysis and non-thermal plasma treatments, Chem. Eng. J. 246 (2014) 184–195, https://doi.org/10.1016/j.cej.2014.02.058.
[21] W. Somers, A. Bogaerts, A.C.T. Van Duin, E.C. Neyts, Plasma species interacting with nickel surfaces: toward an atomic scale understanding of plasma-catalysis, J. Phys. Chem. C 116 (2012) 20958–20965, https://doi.org/10.1021/jp307380w.
[22] C.J. Lee, D.H. Lee, T. Kim, Enhancement of methanation of carbon dioxide using dielectric barrier discharge on a ruthenium catalyst at atmospheric conditions, Catal. Today 293–294 (2017) 97–104, https://doi.org/10.1016/j.cattod.2017.01.022.
[23] E.K. Gibson, C.E. Stere, B. Curran-McAteer, W. Jones, G. Cibin, D. Gianolio, A. Goguet, P.P. Wells, C.R.A. Catlow, P. Collier, P. Hinde, C. Hardacre, Probing the role of a non-thermal plasma (NTP) in the hybrid NTP catalytic oxidation of methane, Angew. Chemie Int. Ed. 56 (2017) 9351–9355, https://doi.org/10.1002/anie.201703550.
[24] T. Nozaki, T. Hiroyuki, K. Okazaki, Hydrogen enrichment of low-calorific fuels using barrier discharge enhanced Ni/γ-Al_2O_3 bed reactor: thermal and nonthermal effect of nonequilibrium plasma, Energy Fuels 20 (2006) 339–345, https://doi.org/10.1021/ef050141s.
[25] Q.H. Trinh, S.B. Lee, Y.S. Mok, Removal of ethylene from air stream by adsorption and plasma-catalytic oxidation using silver-based bimetallic catalysts supported on zeolite, J. Hazard. Mater. 285 (2015) 525–534, https://doi.org/10.1016/j.jhazmat.2014.12.019.
[26] H.-H. Kim, J.-H. Kim, A. Ogata, Microscopic observation of discharge plasma on the surface of zeolites supported metal nanoparticles, J. Phys. D Appl. Phys. 42 (2009), https://doi.org/10.1088/0022-3727/42/13/135210 135210.
[27] X. Tu, H.J. Gallon, J.C. Whitehead, Transition behavior of packed-bed dielectric barrier discharge in argon, IEEE Trans. Plasma Sci. 39 (2011) 2172–2173, https://doi.org/10.1109/TPS.2011.2160289.
[28] S. Pradhan, A.S. Reddy, R.N. Devi, S. Chilukuri, Copper-based catalysts for water gas shift reaction: influence of support on their catalytic activity, Catal. Today 141 (2009) 72–76, https://doi.org/10.1016/j.cattod.2008.06.026.
[29] M.-F. Luo, Y.-J. Zhong, X.-X. Yuan, X.-M. Zheng, TPR and TPD studies of CuO/CeO_2 catalysts for low temperature CO oxidation, Appl. Catal. A Gen. 162 (1997) 121–131, https://doi.org/10.1016/S0926-860X(97)00089-6.
[30] S.S.-Y. Lin, H. Daimon, S.Y. Ha, Co/CeO_2-ZrO_2 catalysts prepared by impregnation and coprecipitation for ethanol steam reforming, Appl. Catal. A Gen. 366 (2009) 252–261, https://doi.org/10.1016/j.apcata.2009.07.010.
[31] W.-C. Chung, K.-L. Pan, H.-M. Lee, M.-B. Chang, Dry reforming of methane with dielectric barrier discharge and ferroelectric packed-bed reactors, Energy Fuels 28 (2014) 7621–7631, https://doi.org/10.1021/ef5020555.
[32] E.C. Neyts, A. Bogaerts, Understanding plasma catalysis through modelling and simulation—a review, J. Phys. D Appl. Phys. 47 (2014), https://doi.org/10.1088/0022-3727/47/22/224010 224010.
[33] J.H. Kwak, L. Kovarik, J. Szanyi, CO_2 reduction on supported Ru/Al_2O_3catalysts: Cluster size dependence of product selectivity, ACS Catal. 3 (2013) 2449–2455, https://doi.org/10.1021/cs400381f.
[34] E. Habenschaden, J. Küppers, Evaluation of flash desorption spectra, Surf. Sci. Lett. 138 (1984) L147–L150, https://doi.org/10.1016/0167-2584(84)90346-3.
[35] Q. Pan, J. Peng, S. Wang, S. Wang, In situ FTIR spectroscopic study of the CO_2 methanation mechanism on $Ni/Ce_{0.5}Zr_{0.5}O_2$, Catal. Sci. Technol. 4 (2014) 502–509, https://doi.org/10.1039/C3CY00868A.
[36] P.A.U. Aldana, F. Ocampo, K. Kobl, B. Louis, F. Thibault-Starzyk, M. Daturi, P. Bazin, S. Thomas, A.C. Roger, Catalytic CO_2 valorization into CH_4 on Ni-based ceria-zirconia. Reaction mechanism by operando IR spectroscopy, Catal. Today 215 (2013) 201–207, https://doi.org/10.1016/j.cattod.2013.02.019.
[37] S. Saeidi, N. Aishah, S. Amin, M.R. Rahimpour, Hydrogenation of CO_2 to value-added products—a review and potential future developments, Biochem. Pharmacol. 5 (2014) 66–81, https://doi.org/10.1016/j.jcou.2013.12.005.
[38] F. Ocampo, B. Louis, L. Kiwi-Minsker, A.C. Roger, Effect of Ce/Zr composition and noble metal promotion on nickel based $Ce_xZr_{1-x}O_2$ catalysts for carbon dioxide methanation, Appl. Catal. A Gen. 392 (2011) 36–44, https://doi.org/10.1016/j.apcata.2010.10.025.